Karlsruher Institut für Technologie

Evaluation of crack profiles by Bando et al.

-Application of COD-results from FE computations

T. Fett, K.G. Schell, C. Bucharsky, G. Rizzi

KIT SCIENTIFIC WORKING PAPERS 152

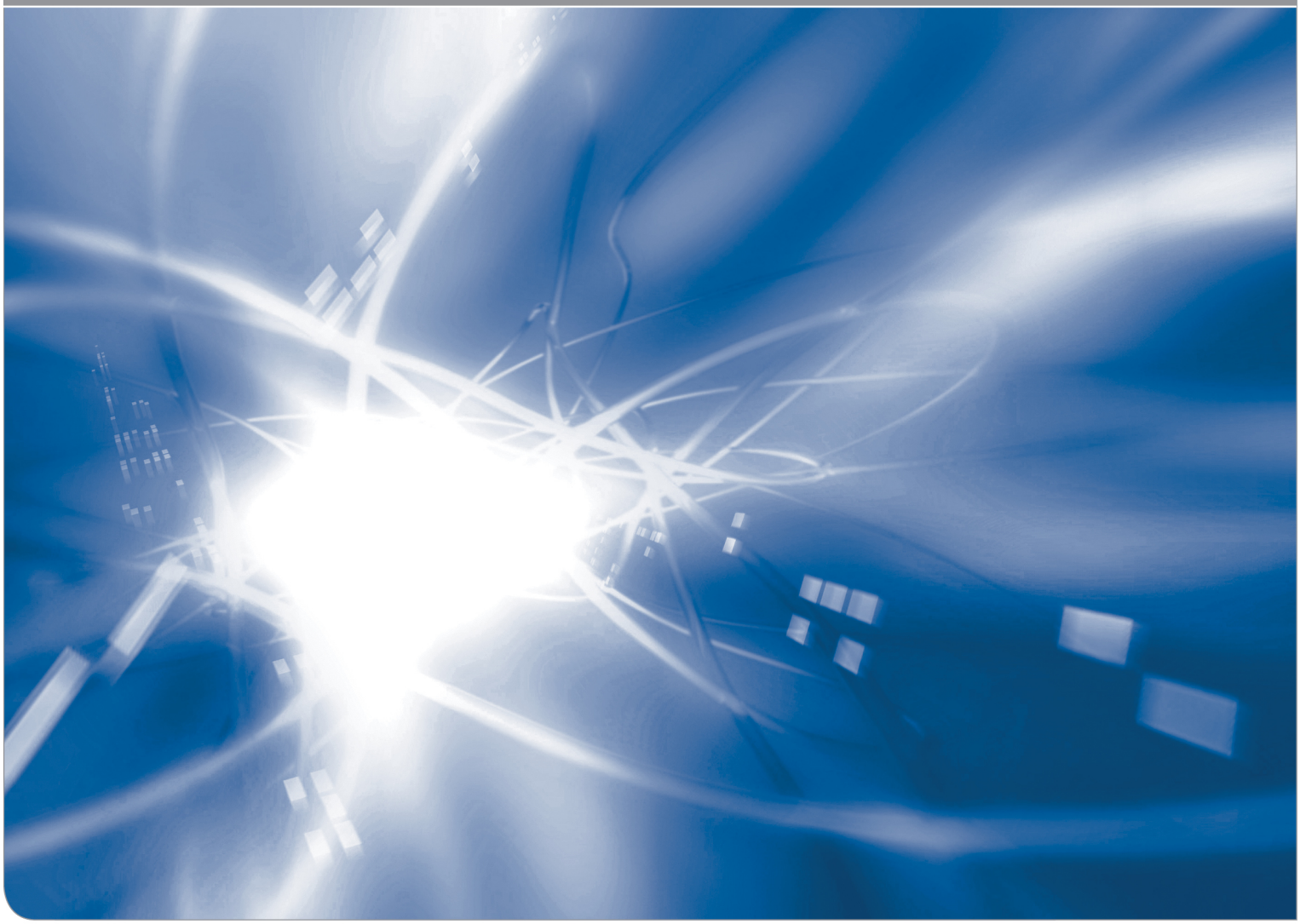

KIT – Universität des Landes Baden-Württemberg und nationales Forschungszentrum in der Helmholtz-Gemeinschaft

IAM Institute for Applied Materials

Impressum

Karlsruher Institut für Technologie (KIT)
www.kit.edu

2020

ISSN: 2194-1629

Abstract

In an earlier Report we dealt with COD-measurements on water-soaked cracks as are available from literature. In this early note, the effect of damage by the water-glass reaction was addressed and for the COD-field the J-integral was adopted for zones ahead of a crack tip showing an elastic module different from that of the bulk. In the present study we apply results of Finite Element (FE) computations to the same problem.

From our FE-computations on crack-flank displacements it was found that the effect of a reduced Young's modulus is visible only in a crack-tip distance as is comparable with the height of the crack-tip zones.

The purely elastic calculations by FE lead to COD profiles, which seem to result in a blunting behavior. This suggests a typical elastic-plastic material behavior to the viewer.

Contents

1 Experimental observations

Since many years, the deformation behaviour at crack tips in silica is discussed controversially. On the one hand, the behavior is described purely elastic. On the other hand, plastic and viscous behavior is assumed. As an argument for the second interpretation the crack opening behaviour measured by Bando et al. [1] on thin lamellas is given. In their paper the authors show profiles of cracks under load which were produced in thin silica sheets of 20-40 nm thickness.

Two of the images by Bando et al. [1] show cracks which were damaged in air and rather rapidly transferred into the TEM-device. The crack profiles are re-plotted in Fig. 1a. Often there is confusion between the total crack opening (total distance of opposite crack faces) and the crack surface displacements (shift of a surface from that in an unloaded state), denoted as COD. That means: When COD is v, crack opening is $2v$.

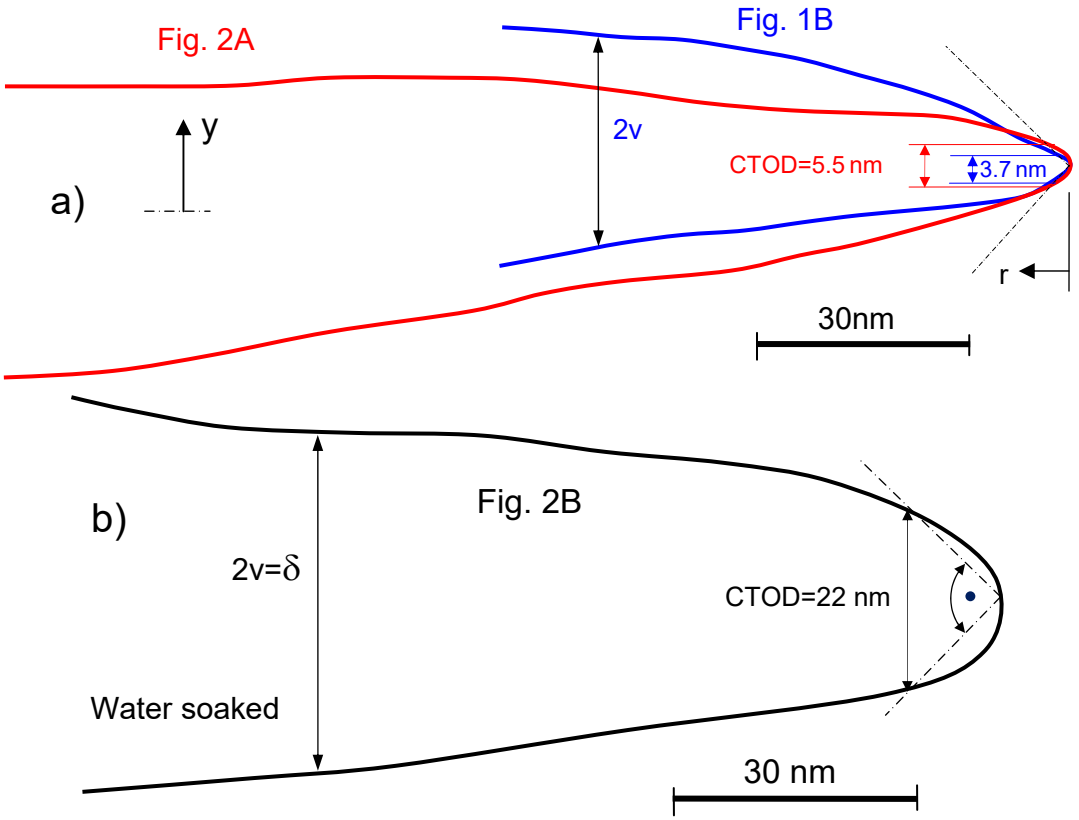

Fig. 1 a) Crack profiles for the two cracks generated in normal lab air according to Figs. 1B (blue profile) and 2A (red profile) of [1], b) profile for long-time water-soaked specimen, Fig. 2B.

A third specimen was cracked with a needle and then soaked for 7 days in water of 90°C. The observed crack-profile is shown in Fig. 1a. From this profile, Bando et al. [1] claimed that crack-tip blunting would occur at the tip. For an explanation of their

blunting effect, they discussed a process of dissolution and precipitation, depending on the local curvature.

Very early this conclusion was questioned by Lawn et al. [2]. It was shown by these authors that an evaluation of crack opening displacements via the Irwin parabola results for the unsoaked specimen in an impossibly high stress intensity factor which was by a factor of 3-4 larger than the fracture toughness of K_{Ic}=0.8 MPa$\sqrt{m}$. Similar argumentation holds for the other cracks, too.

The near-tip solution for the displacements (counted from the symmetry line to the crack surface), the so-called Irwin parabola,

$$v = \sqrt{\frac{8}{\pi}\frac{K}{E}\sqrt{r} + O(r^{3/2})} \tag{1.1}$$

suggests linearity of the plots v^2=f(r) with the slope resulting in K.

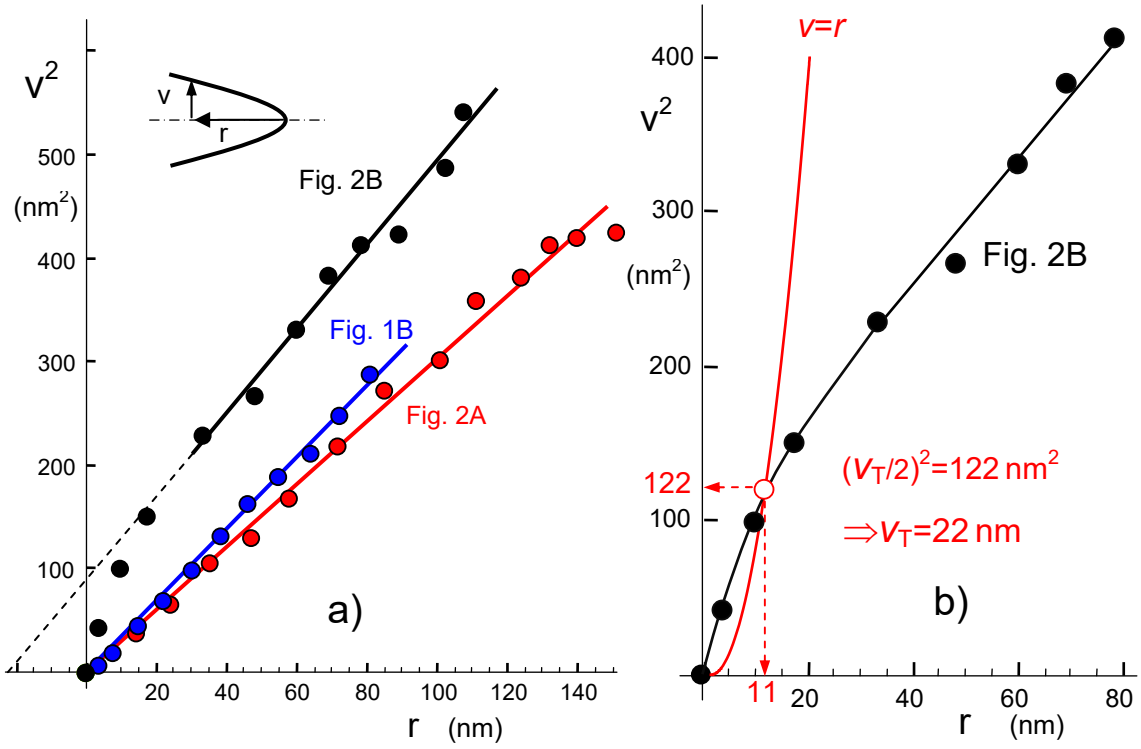

Fig. 2 a) Square of crack-surface displacements in dependence of the crack-tip distance, measurements by Bando et al. [1], b) Determination of Crack-Tip Opening Displacement CTOD as twice the displacements at r=v.

Lawn et al. [2] evaluated COD of a crack in air and obtained over the distance of 150 nm from the crack tip a stress intensity factor of

$$K = 2.7 \pm 0.2 \text{ MPa}\sqrt{\text{m}} \tag{1.2}$$

In Fig. 2a the squares of the displacements, v^2, are plotted versus the crack tip distance r for all cracks. From linear regression it results for the tests in air (90% CI in brackets)

$$K_{1B} = 2.65[2.62, 2.68]\text{MPa}\sqrt{\text{m}} \tag{1.3}$$

$$K_{2A} = 2.48[2.45, 2.51]\text{MPa}\sqrt{\text{m}} \tag{1.4}$$

and for the water-soaked crack

$$K_{2B} = 2.87[2.69, 3.04]\text{MPa}\sqrt{\text{m}} \tag{1.5}$$

The stress intensity factors obtained from the displacements are all in good agreement with each other and agree with the result by Lawn et al. [2]. Whereas the fitted straight lines seem to disappear at $r = 0$ for profiles Fig. 1B, Fig. 2A, the origin of profile Fig. 2B indicates a shift of the crack origin into the bulk material by $\Delta a = 22$ nm and the offset of the asymptotes at r=0 is $v^2 \approx 90$ nm^2.

The crack-tip opening displacement CTOD is defined as twice the displacement at r=v. This condition is introduced in Fig. 2b by the red parabola (note that ordinate is divided into squares of displacements). It results CTOD=22.2 nm.

2 Heart-shaped crack-tip zones

2.1 Zone shape

The singular hydrostatic near-tip stresses are given as

$$\sigma_h = \tfrac{2}{3}(1+\nu)\frac{K}{\sqrt{2\pi r}}\cos(\varphi/2) \tag{2.1}$$

where r and φ are the polar coordinates with the origin at the crack tip, see Fig. 1a. The high hydrostatic crack-tip stresses by eq.(2.1) imply that in the high crack-tip stress field nearly all water is present in form of hydroxyl *S*.

The shape $r(\varphi)$ of the zone contour for constant σ_h in plane strain results from eq.(2.1) as

$$r = \frac{8}{3\sqrt{3}}\omega\cos^2(\theta/2) \tag{2.2}$$

with the height ω of the zone for a prescribed hydrostatic stress

$$\omega = \frac{(1+\nu)^2}{4\sqrt{3}\pi}\left(\frac{K_I}{\sigma_h}\right)^2 \tag{2.3}$$

The contour of constant hydrostatic stress according to eqs.(2.2, 2.3) is shown in Fig. 3a as the heart-shaped contour. This contour also describes the damage zone in front of

the tip of a crack that has not yet grown by subcritical or stable crack growth. Figure 3b illustrates the modulus distribution replaced by an effective constant value.

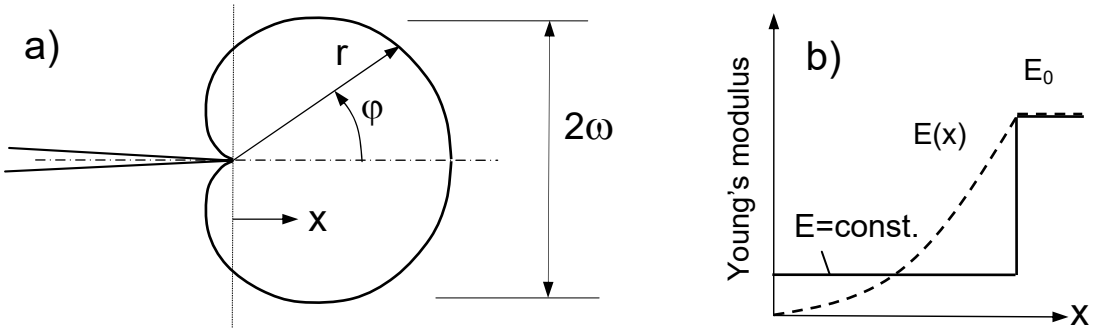

Fig. 3 a) Contour for a constant hydrostatic stress ahead of a loaded crack, b) variation of Young's modulus in a frontal zone $E(x)$ (dashed curve), replaced by an average (effective) modulus E.

2.2 Results from FE computations

Figure 4a shows for example the COD^2-profiles for E/E_0=0.1 obtained via FE-Method as compiled in [3] for heart-shaped zones. The normalized displacements v' represented in Fig. 4 are defined by

$$v' = v \frac{E_0}{K(E_0)\sqrt{\omega}(1-\nu^2)} \tag{2.4}$$

where $K(E_0)$ denotes the stress intensity factor for the case of homogeneous material.

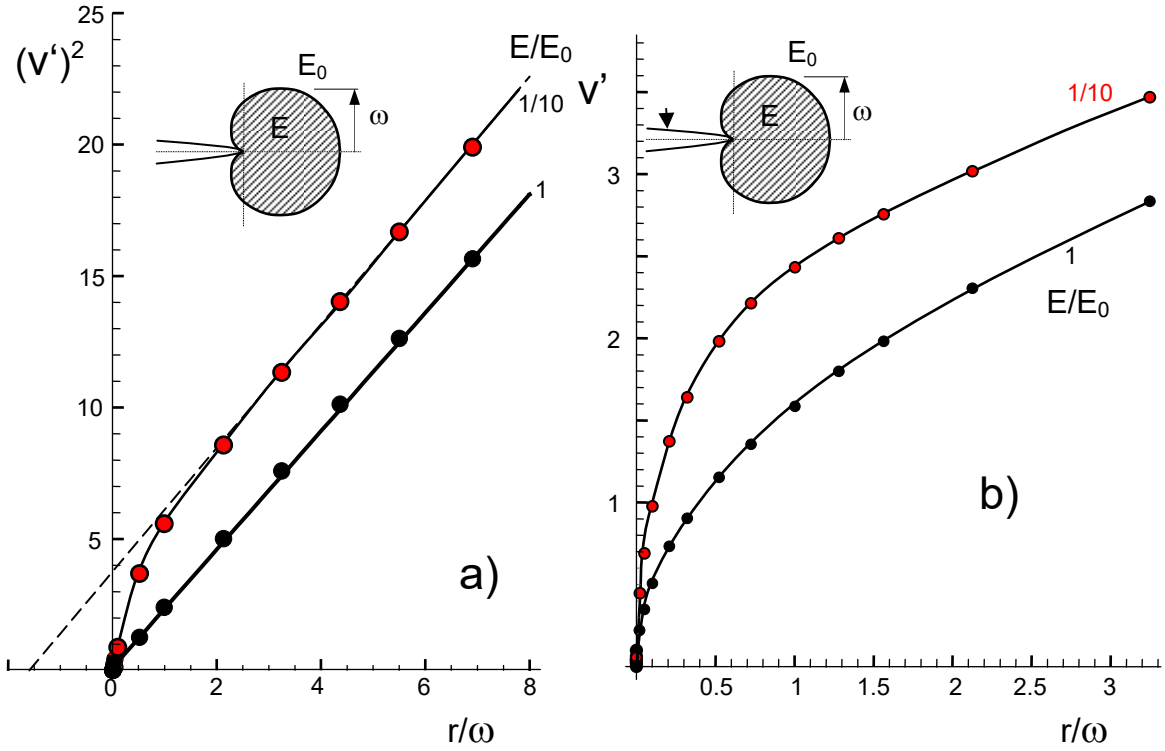

Fig. 4 a) FE-results for normalized COD from [3], b) linear representation of the COD.

In Fig. 4b, the crack-opening displacements of Fig. 4a were plotted again in linear ordinate scaling. Attention should be drawn to the striking correspondence between the calculated profile in Fig. 4a and the measured curve for Fig. 2B [1] in Fig. 2a.

2.3 Consequences of damage on stress intensity factor

At crack tips under externally applied loads, the singular stresses must result in high hydroxyl concentrations and, consequently, high damage. This damage causes a reduction of Young's modulus.

For a theoretical analysis, we prefer for this COD problem the modelling by the heart-shaped zone of reduced modulus since there are two main sources that cause compressive stresses in the crack wake, where no singular stress field is present:

1) In the crack wake the only stress caused by mechanical loading is the so-called *T*-stress. This stress, acting parallel to the crack faces, is negative for specimens loaded by splitting forces (see e.g. Chapter C5.3 in [4]) as were used in the tests by Bando et al. [1].
2) Silica reacting with water shows a volume increase [5]. Since the bulk material will not expand, free expanding of the swollen zones is mechanically restricted and, consequently, water-affected layer are under compressive stresses.

Following the suggestion by Lemaitre and Sermage [6], reduction of Young's modulus under compression is rather small (about 20% of the modulus reduction in comparison with tension). This makes clear that the reduction of Young's modulus is negligible in the crack wake. Consequently, the crack-tip zone with its significant module reduction is roughly heart-shaped. This zone shape will exclusively be considered in the following computations.

The problem of different modulus at the tip and in the bulk material has been studied in [3] via FE-computations and a theoretical analysis by Merkle [7] using the path-independence of the J-Integral by Rice [8].

In a micro-structurally motivated approach, the crack tip region is considered as a slender notch with root radius ρ in the order of the average radius of the SiO_2 rings. For such a notch, Wiederhorn et al. [9] suggested a crack-tip radius of $\rho = 0.5$ nm. The finite crack-tip radius ensures also finite stresses at the tip and finite Young's moduli. The notch intensity that must approach the sharp crack is

$$K_n = K_{appl}\sqrt{\frac{E}{E_0}} \tag{2.5}$$

This result is in rather good agreement with our FE-results in [10] for the case of $0.1 \le E/E_0 \le 1$. Whereas the result by Merkle [7] holds for the limit case of the zone

height and the zone length much smaller than crack length and plate dimensions, modeling by FE must of course violate this basic requirement a priori.
Figure 5a shows the square of the opening displacements at r=0 as a function of Young's modulus in the form $(v')^2_{r=0}=f(E/E_0)^{1/2}$ and Fig. 5b represents the slopes of normalized displacements vs. $(E/E_0)^{1/2}$.

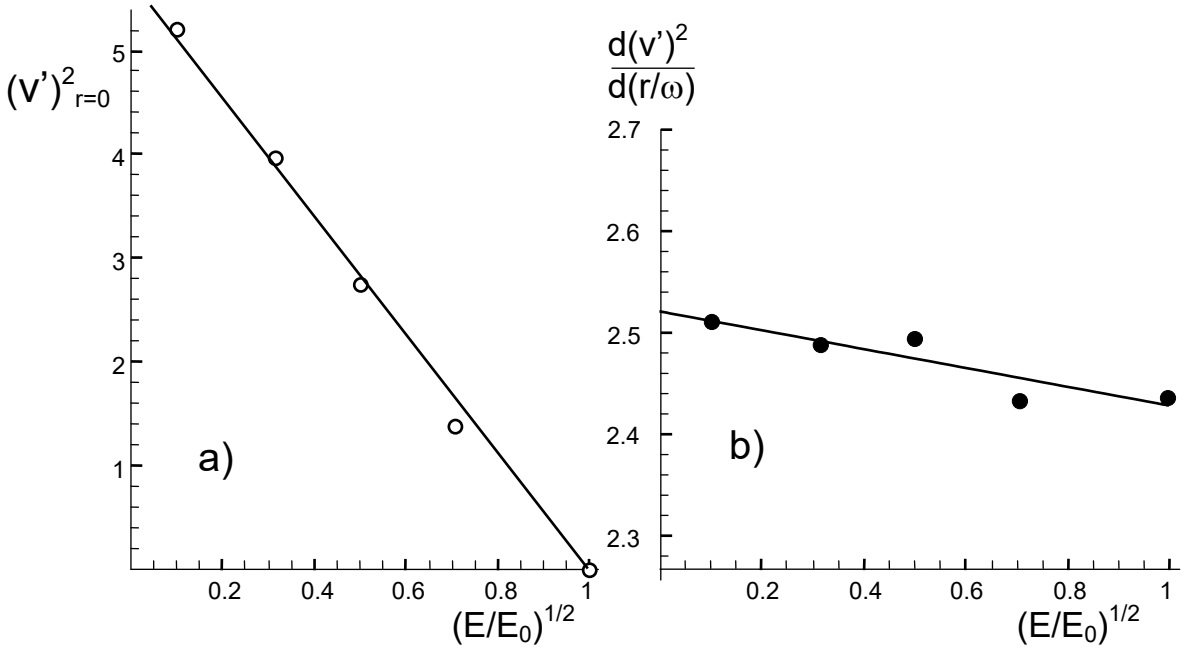

Fig. 5 a) Displacements as a function of Young's modulus in the heart-shaped crack-tip zone, b) slope of the COD straight-lines vs. Young's modulus.

Least-squares fit of Figs. 5a and 5b yield for the square of the opening displacemens

$$(v')^2_{r=0} \cong 5.68\left(1-\left(\frac{E}{E_0}\right)^{1/2}\right)=5.68\left(1-\left(\frac{K}{K(E_0)}\right)\right) \tag{2.6}$$

and for the slopes

$$\frac{d(v')^2}{d(r/\omega)}=2.52-0.092\left(\frac{E}{E_0}\right)^{1/2}\approx 2.47\pm 0.035 \tag{2.7}$$

with the last number standing for ±1 Standard Deviation.

3 Evaluation of experimental results

As Lawn et al. [2] aptly mentioned, the cracks in the glass lamellas must have grown subcritically in the region of higher crack velocities. Figure 6 shows subcritical crack-growth rates by [11]. Assuming a crack rate of $da/dt=10^{-7}$ m/s, at room temperature, a

K-value of about 0.48 MPa√m can be concluded (blue arrows) and for 90°C (red arrow) K≈0.43 MPa√m is expected.

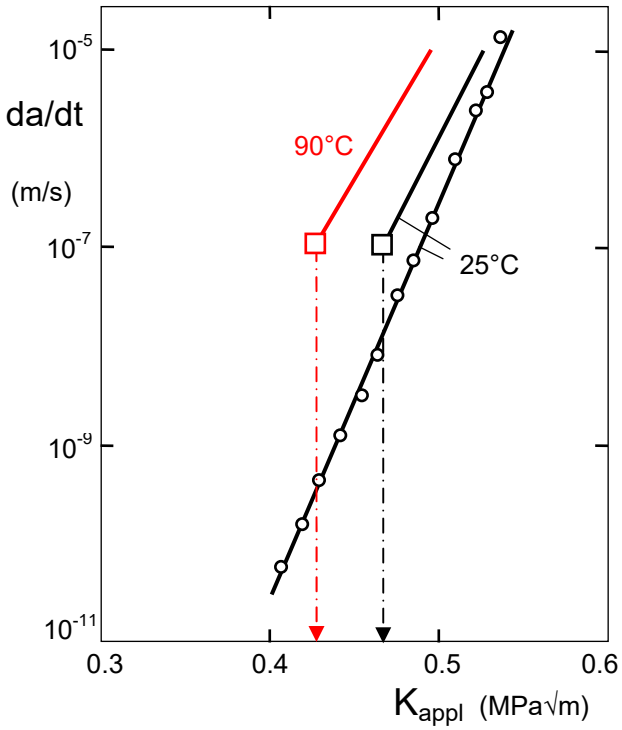

Fig. 6 Subcritical crack growth curves of silica in liquid water by Wiederhorn and Bolz [11].

As mentioned before, the stress intensity factor during subcritical crack growth is at test temperature about K≈0.43 MPa√m for water-soaked and K≈0.47 MPa√m for freshly fractured specimens as is illustrated by the arrows in Fig. 6. The apparent stress intensity factors $K(E_0)$ obtained by an evaluation via E=E_0=72 GPa (assuming an un-damaged glass) resulted for the freshly damaged state according to eqs.(1.2-1.4) in $K(E_0)$≈2.6 MPa√m and, consequently

$$E = \left(\frac{K}{K(E_0)}\right)^2 E_0 \approx \left(\frac{0.47}{2.6}\right)^2 72\,\text{GPa} \cong 2.35\,\text{GPa} \tag{3.1}$$

for the specimen soaked at 90°C, and $K(E_0)$≈2.87 MPa√m one obtains in the same way

$$E \approx \left(\frac{0.43}{2.87}\right)^2 72\,\text{GPa} \cong 1.6\,\text{GPa} \tag{3.2}$$

These Young's moduli enable to compute the normalized crack-opening displacement from v' from eq.(2.4). In the latter case we find from eqs.(2.4) and (3.1)

$$v'_{r=0} \cong 2.38\left(1-\left(\frac{E}{E_0}\right)^{1/2}\right)^{1/2} = 2.38\left(1-\frac{K}{K(E_0)}\right)^{1/2} = 2.2 \qquad (3.3)$$

From eqs.(3.1) and (3.2) we can compute the height of the heart-shaped zones with reduced Young's modulus E. For the water-soaked cracked glass lamella we have

$$K(E)\approx 0.43 \text{ MPa}\sqrt{\text{m}},\ K(E_0)\approx 2.87 \text{ MPa}\sqrt{\text{m}},\ (v)^2=90 \text{ nm}^2,$$
$$\text{and, consequently } v=9.5 \text{ nm}$$

From eq.(2.4) and the definition of the normalized crack-opening displacement by eq.(1.6), it yields

$$\omega = \left(\frac{v\,E_0}{K(E_0)v'(1-\nu^2)}\right)^2 \qquad (3.4)$$

with the result of **$\omega\approx$12.5 nm**. Without wanting to overestimate the scattering behavior of the data in Fig. 2, we can conclude that the offset of curves 1B and 2A is certainly less than 10% of straight line 2B. This would lead to an upper limit of $v < 3.2$ nm or via (3.4) in roughly **$\omega <$ 1.5 nm**.

The large differences in the heights of the heart-shaped zones is predominantly caused by an important geometrical difference in specimen properties. In normally used fracture mechanics test specimens, the water-containing zone ahead of a crack-tip develops by diffusion with a diffusion length of

$$b = \sqrt{Dt} \qquad (3.5)$$

where D stands for the diffusivity of water in silica and t for the time. Thin sheets in the order of B=20-40nm thickness, which are water-soaked for 7 days at 90°C must show a stationary water concentration distribution. The reason is that water can diffuse from the two side surfaces (Fig. 7).

The diffusivity is according to Zouine et al. [12] $D \approx 3\ 10^{-19}\text{m}^2/\text{s}$. With $t = 7$ days $= 6\times10^5$s it results: $b \approx 400$ nm. This is much more than the half sheet thickness of $B/2 =$ 10-20 nm. Therefore, any diffusion effects can be ignored and the diffusion zone can always be viewed as fully developed.

When a crack grows after load application in normal air as the environment, the same effect will occur as considered before but now with a reduced extend. Since the time between crack generation and observation under the TEM is rather short, the diffusion length b is clearly smaller.

For an estimated time span of specimen contact with humid air between introducing the needle into the foil and evacuation in the TEM of only 60 s and a diffusivity at room temperature (23°C) of $D_0 = 10^{-21}\text{m}^2/\text{s}$, nearly negligible diffusion depths of about 0.25 nm from the side surfaces into the bulk material have to be expected.

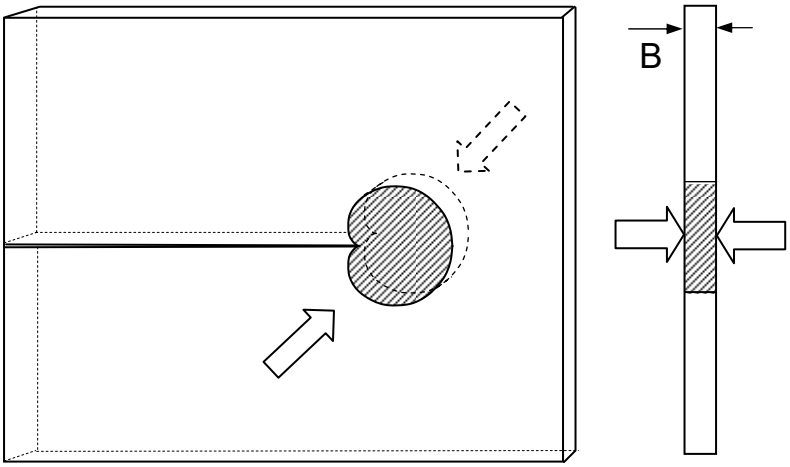

Fig. 7 Thin sheet of silica soaked with water from the side surfaces.

References

1 Y. Bando, S. Ito, M. Tomozawa, Direct Observation of Crack Tip Geometry of SiO_2 Glass by High-Resolution Electron Microscopy, J. Am. Ceram. Soc., **67** (1984), C36 C37.

2 B.R. Lawn, D.B. Marshall, A.H. Heuer, Comment on "Direct observation of crack tip geometry of SiO_2 glass by high-resolution electron microscopy", J. Am. Ceram. Soc. **67**(1984), C253.

3 G. Rizzi, T. Fett, K.G. Schell, C. Bucharsky, Crack-flank displacements for cracks with zones of reduced Young's modulus, **150**, 2020, ISSN: 2194-1629, Karlsruhe, KIT

4 T. Fett, Stress intensity factors, T-stress, Weight Functions, IKM 50, Universitätsverlag Karlsruhe, 2008.

5 Shelby, J.E., Density of vitreous silica, J. Non-Cryst. **349** (2004), 331-336.

13.6 J. Lemaitre, J.P. Sermage, One damage law for different mechanisms, Comp. Mech., **20**(1997), 84-88.

7 J. G. Merkle, An application of the J-integral to an incremental analysis of blunt crack behavior, Mechanical Engineering. Publications, London, 1991, 319-332.

8 Rice, J.R., A path independent integral and the approximate analysis of strain concentration by notches and cracks, Trans. ASME, J. Appl. Mech. (1986), 379-386.

9 S.M. Wiederhorn, E.R. Fuller, Jr. and R. Thomson, Micromechanisms of crack growth in ceramics and glasses in corrosive environments, Metal Science, **14**(1980), 450-8.

10 G. Rizzi, K.G. Schell, C. Bucharsky, T. Fett, FE-Study on heart-shaped crack-tip zones, **142**, 2020, ISSN: 2194-1629, Karlsruhe, KIT.

11 S.M. Wiederhorn and L.H. Bolz, Stress Corrosion and Static Fatigue of Glass, *J. Am. Ceram. Soc.* **53**[1810] 543-548 (1970).

12 Zouine, A., Dersch, O., Walter, G., Rauch, F., Diffusivity and solubility of water in silica glass in the temperature range 23-200°C, Phys. Chem. Glasses, **48**(2007), 85-91.

KIT Scientific Working Papers
ISSN 2194-1629

www.kit.edu